Geophysical Journal International

Geophys. J. Int. (2020) **0,** 1–0
GJI Seismology

doi: 10.1093/gji/ggaa261

Methodology to identify the reference rock sites in regions of medium-to-high seismicity: an application in Central Italy

Giovanni Lanzano,[1] Chiara Felicetta,[1] Francesca Pacor,[1] Daniele Spallarossa[2] and Paola Traversa[3]

[1] *Istituto Nazionale di Geofisica e Vulcanologia, Via di Vigna Murata, 605, 00143 Rome RM, Italy. E-mail: giovanni.lanzano@ingv.it*
[2] *University of Genova, Via Balbi, 5, 16126 Genoa GE, Italy*
[3] *Électricité de France, France*

Accepted 2020 May 22. Received 2020 May 20; in original form 2019 October 30

SUMMARY

To evaluate the site response using both empirical approaches (e.g. standard spectral ratio, ground motion models (GMMs), generalized inversion techniques, etc.) and numerical 1-D/2-D analyses, the definition of the reference motion, that is the ground motion recorded at stations unaffected by site-effects due to topographic, stratigraphic or basin effects, is needed. The main objective of this work is to define a robust strategy to identify the seismic stations that can be considered as reference rock sites, using six proxies for the site response: three proxies are related to the analysis of geophysical and seismological data (the repeatable site term from the residual analysis, the resonance frequencies from horizontal-to-vertical spectral ratios on noise or earthquake signals, the average shear wave velocity in the first 30 m); the remaining ones concern geomorphological and installation features (outcropping rocks or stiff soils, flat topography and absence of interaction with structures). We introduce a weighting scheme to take into account the availability and the quality of the site information, as well as the fulfillment of the criterion associated to each proxy. We also introduce a hierarchical index, to take into account the relevance of the proposed proxies in the description of the site effects, and an acceptance threshold for reference rock sites identification. The procedure is applied on a very large data set, composed by accelerometric and velocimetric waveforms, recorded in Central Italy in the period 2008–2018. This data set is composed by more than 30 000 waveforms relative to 450 earthquakes in the magnitude range 3.2–6.5 and recorded by more than 450 stations. A total of 36 out of 133 candidate stations are identified as reference sites: the majority of them are installed on rock with flat topography, but this condition is not sufficient to guarantee the absence of amplifications, especially at high frequencies. Seismological analyses are necessary to exclude stations affected by resonances. We test the impact of using these sites by calibrating a GMMs. The results show that for reference rock sites the median predictions are reduced down to about 45 per cent at short periods in comparison to the generic rock motions.

Key words: Earthquake ground motions; Seismic attenuation; Site effects.

INTRODUCTION

In order to evaluate the site response using empirical approaches (e.g. standard spectral ratio, ground motion models—GMMs, generalized inversion technics—GIT) and numerical 1-D/2-D analyses, the definition of the reference motion, that is the ground motion recorded at stations unaffected by site-effects, is needed. The common practice is to assume that sites where rocks or stiff soils outcrop and the average shear wave velocity in the uppermost 30 m ($V_{S,30}$) exceeds a given value represent an example of reference sites. In the European seismic code (Eurocode 8–EC8, CEN 2004), this value is set to 800 m s^{-1} (soil category EC8-A), while in the NEHRP provision (BSSC 2003), a distinction is introduced between hard rock, corresponding to $V_{S,30} > 1500$ m s^{-1}, and firm to hard rock for $V_{S,30}$ in the range 760–1500 m s^{-1}.

In the calibration of GMMs, the site amplifications at the different stations are usually evaluated with respect to the predictions of sites with $V_{S,30}$ exceeding or corresponding to a given value (i.e. 760 m s^{-1} for Boore *et al.* 2014 or 800 m s^{-1} for Lanzano *et al.* 2019). However, the simple definition of reference rock sites based only on geological features and measurements of the shear wave profiles, does not ensure to identify sites whose amplification is expected to

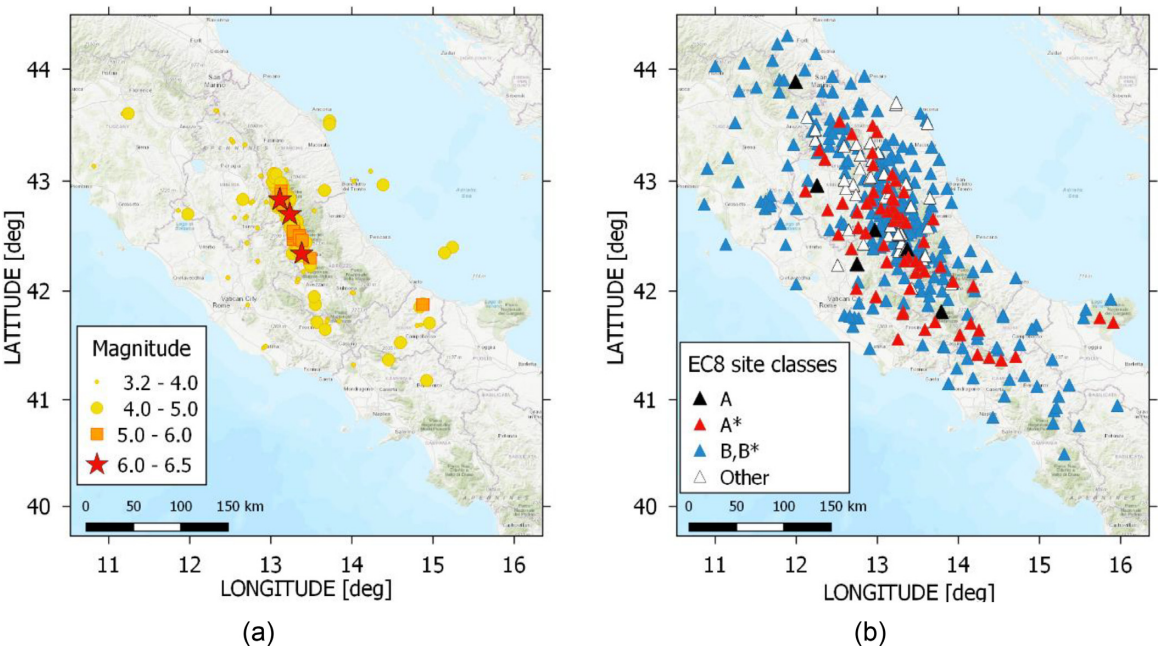

Figure 1. Geographical distribution of epicentres of the events (a) and stations (b) included in the data set.

be negligible. It is well known that alteration or intensive fracturing of rock bodies may significantly modify their mechanical behaviour and, in particular, may be responsible of energy trapping phenomena (Di Naccio *et al.* 2017). Indeed, there are several cases in the literature showing evidence for local amplification with resonance peaks at intermediate and high frequencies at sites having $V_{S,30}$ larger than 800 m s^{-1} (Steidl *et al.* 1996; Rovelli *et al.* 2002; Bindi *et al.* 2009; Marzorati *et al.* 2011; Ktenidou & Abrahamson 2016) or effects of wave polarization (Pischiutta *et al.* 2011; Burjanek *et al.* 2014). As a consequence, an inappropriate selection of reference sites may cause inaccurate prediction of the expected rock motion when hazard is evaluated including site effects, due to the amplified response of the motion. Cadet *et al.* (2010) proposed a procedure to identify a standard reference site based both on $V_{S,30}$ (between 750 and 850 m s^{-1}) and fundamental resonance frequency ($f_0 > 8$ Hz) in order to reduce the variability in the amplitude of the site response and to constrain the amplify frequency band, respectively. Recently, Felicetta *et al.* (2018) proposed a procedure to recognize reference rock sites among the recording stations of the Italian ACcelerometric Archive (ITACA, http://itaca.mi.ingv.it; Luzi *et al.* 2019) using six proxies, based on geological, topographical and geophysical parameters. Three proxies out of six are based on geophysical and seismological data ($V_{S,30}$, horizontal-to-vertical spectral ratios of noise measurements—HVNRS, and response spectra—HVSR), whereas the remaining three are based on geological and geomorphological features (outcropping rock, flat topography and absence of interaction with structures). These proxies were applied to a set of stations classified as EC8-A and formerly used for the calibration of a reference GMM for Italy (ITA10, Bindi *et al.* 2011). The authors showed that such model calibrated for reference rock sites provides median values and associated standard deviations, lower than the ITA10 values, estimated for generic rock sites (EC8-A).

Following the approach proposed by Felicetta *et al.* (2018, FEL18 in the following), the aim of this study is to update and test a set of proxies able to identify recording stations installed on reference rock sites. Differently from FEL18, we sort the six proxies introducing a hierarchical index (HI), variable from 0.5 to 2, to take into account their capability to represent the seismic response of the stations. Furthermore, since information on site response may be limited for large seismic data sets, for each proxy we propose a weighting scheme (PW), variable from 0 to 1, to take into account the presence/absence and the quality of the information. By the combination of hierarchical indexes and weights, we can assign an overall score and identify the reference sites as those that exceed a given threshold.

The procedure is applied to a rich data set of 30 000 records collected in Central Italy in the time interval 2008–2018. In order to reduce the number of investigated sites, we perform a preliminary residual analysis to identify the candidate reference rock sites, evaluating the systematic site term with respect to EC8-A predictions of ITA10. Then, we apply the proposed procedure to rank the stations. Reference rock sites are identified as those that exceed a given threshold. Finally, the impact of this selection procedure is evaluated by means of the calibration of a GMM for reference rock sites. Note that the proposed predictive model is not aimed at updating FEL18, mainly because the data, although very numerous, refer to a local 'training' area and cannot be extended to the whole Italian territory.

DATA SET

The data set used for the analysis was assembled in cooperation with the working group involved in the seismic microzonation study carried out in Central Italy after the 2016 M_w 6.0 Amatrice earthquake (Priolo *et al.* 2019). The collection of records is composed by accelerometric and velocimetric three components waveforms of events located in Central Italy and occurred between 2008 and 2018 (Fig. 1a).

The epicentral distribution of the events is aligned along the extensional system of the active faults in the Apennine chain (Boncio *et al.* 2004 and references therein; Chiaraluce *et al.* 2017; Porreca *et al.* 2018), where most of the historical and instrumental seismicity is located. The focal mechanisms of the strongest events are normal dip-slip with NNW–SSE striking focal planes

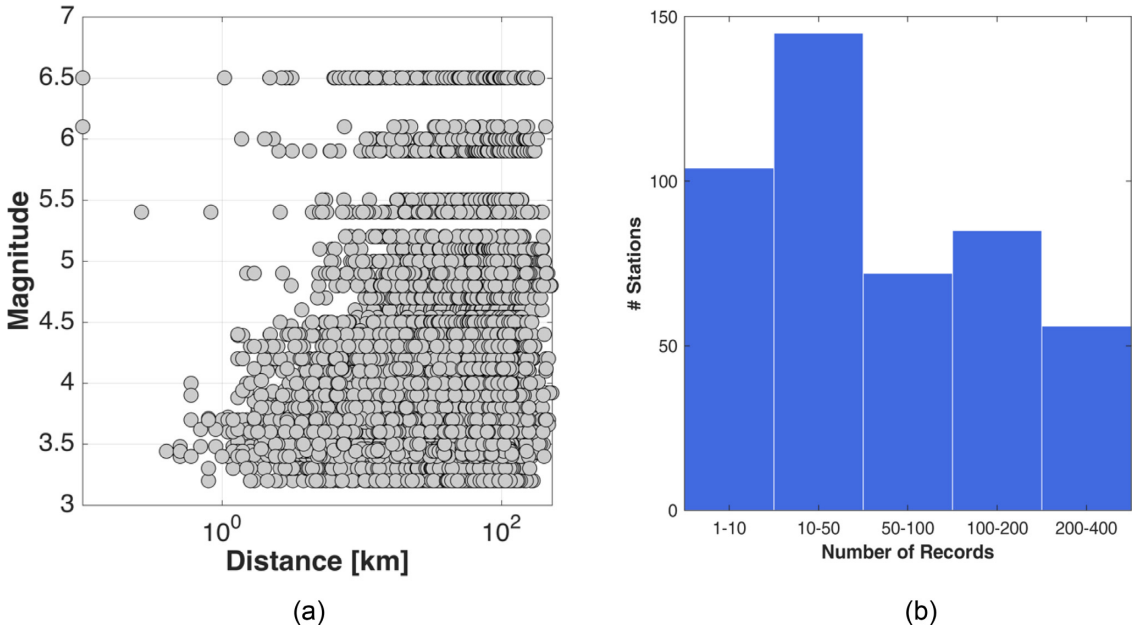

Figure 2. (a) Magnitude–distance scatter plot of the data set. (b) Records sampling of the stations.

(http://cnt.rm.ingv.it/tdmt; Pondrelli *et al.* 2016), compatible with both the kinematics of the main faults and the SW–NE trending tensional stress regime characterizing the regions of Central Italy (Ferrarini *et al.* 2015). The recording stations (Fig. 1b) belong to permanent (RAN—Rete Accelerometrica Nazionale, https://doi.org/10.7914/SN/IT and RSN—Rete Sismica Nazionale, https://doi.org/10.13127/SD/X0FXnH7QfY) and temporary networks, installed to monitor the seismic sequences and to investigate the site effects, after the 2009 L'Aquila (M_w 6.1) and the 2016 Amatrice (M_w 6.0) earthquakes.

The data set is composed by more than 30 000 waveforms relative to about 450 earthquakes in the magnitude range 3.2–6.5 (local magnitude for $M < 4.5$ and moment magnitude for $M \geq 4.5$) recorded by about 460 stations within 250 km from the epicentres (Fig. 1b). For the strongest events ($M > 5.5$), the Joyner and Boore distance (R_{JB}) is adopted and computed from the fault geometries published in the ITACA database (ITalian ACcelerometric Archive; itaca.mi.ingv.it; Pacor *et al.* 2011), whereas for other events the epicentral distance is used. The data set is very well sampled in the distance and magnitude ranges R [10–100] km and M [3.2–4.5]. The large amount of records at short distances and for small events is due to the stations of the temporary networks. About the 75 per cent of the stations have recorded more than 10 events and, in several cases, more than 100 (Fig. 2).

The local site conditions at the recording stations are highly heterogeneous, due to the presence of different morphology (large and narrow alluvial valleys, slopes and mountain peaks) and lithology (e.g. gravel and sand deposits, alluvial terraces, thick debris covers along the slopes) in the area. The site information of the recording stations is extracted from ITACA and microzonation studies carried out in the region (Pagliaroli *et al.* 2019; Pergalani *et al.* 2019). The CRISP (Bordoni *et al.* 2017) repository is also consulted to collect the geological information and the noise measurements of the permanent velocimetric stations belonging to RSN network.

The *S*-wave profile is available for about 10 per cent of the recording stations included in the data set and the EC8 soil category (CEN 2004) is assigned according to the $V_{S,30}$ value. For the remaining stations, the EC8 class is attributed on the basis of the surface geology, inferred from the existing cartography (Fig. 3).

As expected, the majority of the sites is classified as EC8-B (deposits of very dense sand, gravel, or very stiff clay at least several tens of metres in thickness, characterized by a gradual increase of the mechanical properties with depth; $V_{S,30}$ in the range 360–800 m s^{-1}). The EC8-A rock sites, corresponding to $V_{S,30} \geq 800$ m s^{-1} or rock-like geological formation, are about 15 per cent of the selected stations. However, the seismological analyses carried out in Central Italy (Priolo *et al.* 2019) showed that also sites located on rock may present high-frequency amplifications, probably related to a reduction of the stiffness at shallow depths.

SELECTION OF THE CANDIDATE STATIONS BY MEAN OF RESIDUAL ANALYSIS

The selection of the stations candidate to be reference rock sites is carried out via a residual analysis with respect to an existing GMM. The residuals are calculated as the (natural) logarithmic difference between observation and predictions. The GMM, used as reference predictive equation, is that proposed by Bindi *et al.* (2011) for shallow active crustal earthquakes in Italy (ITA10). The analysis is carried out for the geometric mean of the horizontal components of the peak ground acceleration and 69 ordinates of the acceleration response spectra (5 per cent damping) in the period range $T = 0.04$–2 s. The total residuals, R_{es}, are decomposed in between-event (δB_e) and within-event (δW_{es}) terms following the definition adopted in site-specific seismic hazard analyses to relax the ergodic assumption (e.g. Al-Atik *et al.* 2010; Luzi *et al.* 2014; Rodriguez-Marek *et al.* 2014). δB_e is calculated as the mean of the total residuals of each earthquake in the data set and represents the average misfit of the recordings of one particular earthquake with respect to the median ground-motion model. The δB_e and δW_{es} residuals are assumed to be normally distributed with standard deviations τ and φ, respectively. The δW_{es} is further decomposed into site-to-site term ($\delta S2S_s$) and

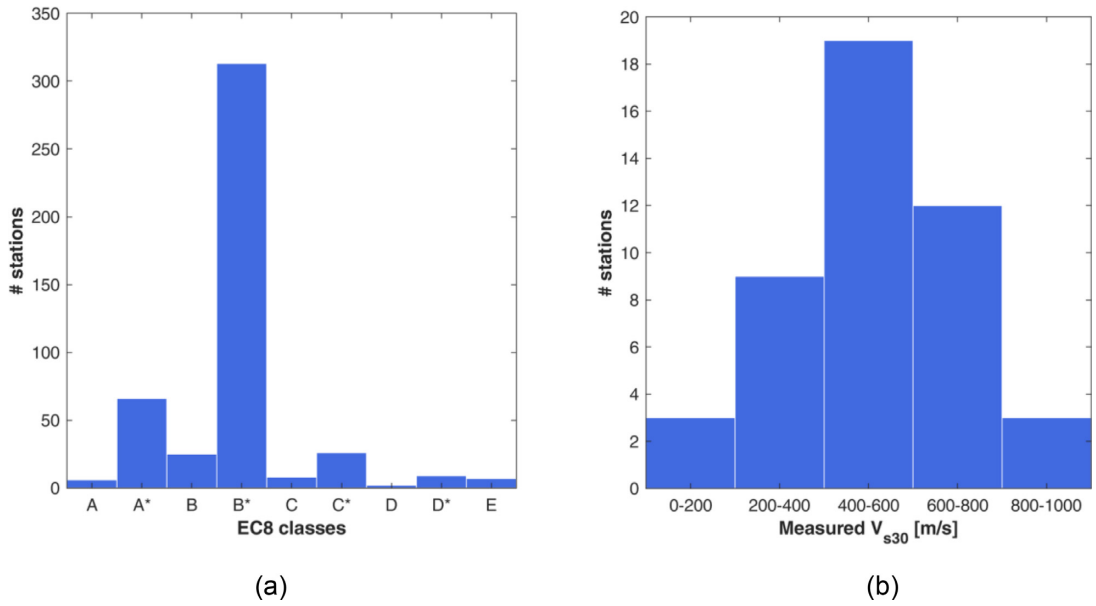

Figure 3. Distribution of EC8 soil categories (a) and measured $V_{S,30}$ (b) in the data set. The asterisk indicates soil categories inferred from surface geology.

event- and site-corrected residual ($\delta W_{0,es}$). $\delta S2S_s$ is calculated as:

$$\delta\ S2S_s = \frac{1}{NE_s} \sum_{e=1}^{NE_s} \delta W_{es} \tag{1}$$

where NE_s is the number of events recorded at the station s. This term quantifies the average misfit of recordings from one particular site with respect to the event-corrected median ground-motion. The event-corrected single-station standard deviation, $\phi_{ss,s}$, is also computed as:

$$\phi_{ss,s} = \sqrt{\frac{\sum_{e=1}^{NE_s} (\delta W_{es} - \delta S2S_s)^2}{NE_s - 1}} \tag{2}$$

For the purpose of this study, the site-to-site term is computed with respect to the reference site category of ITA10, that is the EC8-A class. In this way, the site-to-site term, named $\delta S2S_{\text{EC8-A}}$, can be used as proxy of the empirical amplification of the station.

Our strategy to identify the candidate reference rock sites is based on a cluster analysis over the $\delta S2S_{\text{EC8-A}}$ curves with the aim of detecting the sites with the lowest $\delta S2S_{\text{EC8-A}}$ and flat trend. Other authors have recently applied the cluster analysis as a data-driven tool to categorize sites presenting similar features in their empirical response (Puglia *et al.* 2015; Kotha *et al.* 2018). Starting from the 462 sites of the data set, we perform the cluster analysis on the stations with: (i) the single-station variability $\phi_{ss,s}$ (eq. 2) lower than the within-event variability of ITA10 for the 75 per cent of the considered ground motion parameter and (ii) at least 10 records (according to Lanzano *et al.* 2017).

The map of the stations is reported in Fig. 4: 119 (25 per cent) sites, mainly located at the border of the investigated area, are disregarded for the cluster analysis.

Among several techniques for data aggregation available in literature, we use the *k*-means clustering (David & Vassilvitskii 2007) to partition the observations of the *n*-by-*p* $\delta S2S_{\text{EC8-A}}$ matrix into *k* clusters, where *n* is the number of sites and *p* is the number of parameters. The main advantage of this method is that it converges very quickly; the drawback is that the number of clusters must be assigned *a priori*.

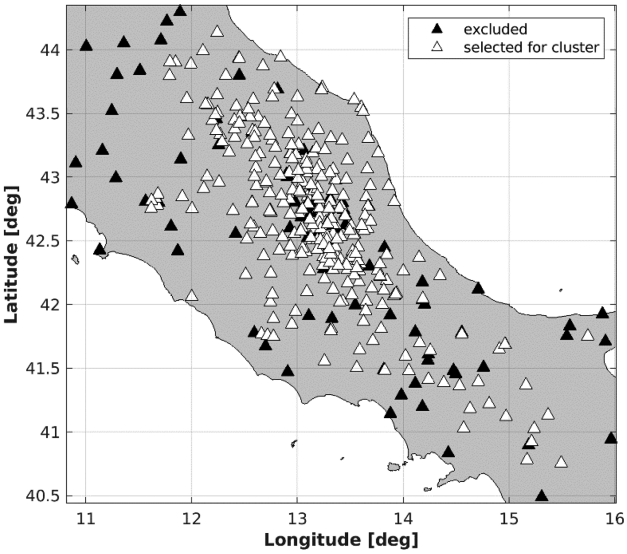

Figure 4. Stations selected for the cluster analysis.

After some trial analyses, nine clusters of $\delta S2S_{\text{EC8-A}}$ curves were considered, allowing to clearly identify classes including the candidate stations as reference rock sites (Fig. 5). In particular, we want to distinguish classes representative of sites presenting flat trend and de-amplifications from sites presenting flat trend and zero-amplification (with respect to the mean prediction of rock sites of the reference GMM). Since the main target of the analysis is the detection of these classes, possible redundancies in the clustering of the sites presenting amplifications are allowed.

The cluster #1 contains stations characterized by a de-amplification and a quite flat trend at all periods (Fig. 6a); while the cluster #6 exhibits, on average, zero amplification at all periods, that is it includes sites having a mean ground motion response very similar to those predicted by ITA10 for EC8-A (Fig. 6b). All other classes show clear amplification effects, ($e^{\delta S2S} > 1$) in different frequency bands.

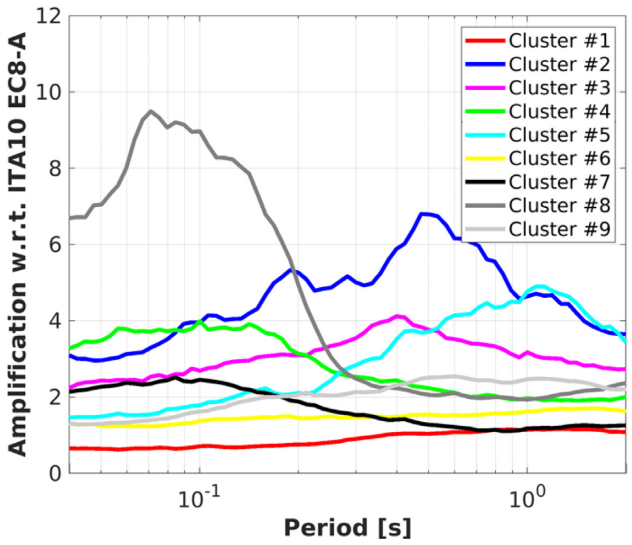

Figure 5. Mean amplification ($e^{\delta S2S}$) of the clusters after the *k*-means clusterization.

The cluster #1 is composed by 72 stations: 54 of cluster #1 are within the confidence interval, corresponding to 75 per cent of the total number of stations in the cluster. The cluster #6 is instead composed by 61 stations and 36 are within the confidence interval (60 per cent).

Among the stations not clustered in #1 and #6, 31 sites are classified as EC8-A, confirming that several rock sites may exhibit significant site-effects: for most of the sites (30/31), the soil category has been inferred from proxies (surface geology or $V_{S,30}$ from topography), but, in the case of station AQP, an *in situ* measurement of $V_{S,30}$ is available (836 m s^{-1}). As a matter of fact, the latter station shows intermediate-to-long periods amplifications with f_0 around 2 Hz and its behaviour can be ascribed to topographic effect, since it is installed on a ridge with flat crest and very steep flanks (http://itaca.mi.ingv.it/ItacaNet_31/#/station/IT/AQP).

PROXIES AND WEIGHTING SCHEME

The rationale of the proposed approach to recognize reference sites, is derived from the decision-matrix method (DMM), named also Pugh method (Pugh 1981). DMM is a qualitative technique used to rank the multidimensional options of an option set. A basic decision matrix consists of establishing a set of criteria which are scored and summed up to gain a total score which can then be ranked. A weighted decision matrix operates in the same way as the basic decision matrix but introduces the concept of weighting the criteria in order of importance.

Starting from the analysis of FEL18, we define six proxies to identify reference rock sites, based on geological, topographical, geophysical and seismological indicators. Differently from FEL18, we introduce a weighting scheme to handle the relevance, the data quality and the possible lacking of these indicators. The weighting scheme is given by the combination of two indexes (HI and PS): the former expresses the importance of the proxy in representing the site effect, the latter evaluates the degree of fulfillment of the acceptance criterion for each proxy. By means the application of the weighting scheme to the stations belonging to cluster #1 and cluster #6, we award a final ranking of the candidates to be reference sites. The proposed proxies and the acceptance criteria are listed in Table 1, while the assigned weights and scores are listed in Table 2.

Two proxies out of six are based on seismological data (H/V and $\delta S2S$), whereas the remaining four rely on geophysical, geological, geomorphological and installation features ($V_{S,30}$, GEO, TOP and HOU). The proposed proxies (or a combination of these proxies) were already satisfactorily used to verify that there are no site-effects at rock stations (Felicetta *et al.* 2018: Luzi *et al.* 2019; Priolo *et al.* 2019). Indeed, these site parameters can be easily obtained in contexts of medium-high seismicity, where data sets rich in recordings are available, many stations are installed, geological maps are available throughout the entire territory and many sites are characterized by geophysical tests.

First, we assign a weight to the proxy values (PW, listed in Table 2), on the base of following general rules:

1 If the criterion is met, the weight is set equal to 1.
2 If the proxy value does not fulfill the requirement, the weight is set equal to 0.
3 If no information is available for the proxy, the weight is set equal to 0.
4 When the criteria are partially met, the weights may range from 0.25 to 0.75.

Then, because of the different capability of the selected proxies to represent the seismic response of the stations, we first introduce a HI, variable from 0.5 to 2 (Table 2). We assume that the most important indicators for site-effect characterization are the surface geology (GEO), the $V_{S,30}$ and the HV from Fourier spectra, as also indicated by recent results of the task devoted to the site effects in the SERA project 2017–2020 (Cultrera *et al.* 2019), while HOU and TOP are considered less relevant for the purpose. Finally, the score assigned to each proxy is given by the product of HI and PW. The complete fulfillment of the criteria in Table 2 defines the ideal reference rock site and corresponds to total score of 8.

In the following, we provide a short description of the selected proxies and the associated acceptance criteria

Housing—HOU

Many studies show that records of stations located inside or close to buildings may be affected by the vibrations of the structure as well as by soil-structure interaction phenomena (Stewart *et al.* 1999; Gallipoli *et al.* 2004). In Italy, several accelerometric stations of the RAN network are not in free-field conditions, since they are located in electrical transformation cabins (Gorini *et al.* 2010). However, their influence is limited at specific frequencies, usually larger than 5 Hz (Ditommaso *et al.* 2010).

To remove stations with possible dynamic interaction effects, we introduce the proxy housing (HOU), which indicates where the recording station is installed. Its weight is PW = 1 for free-field stations and PW = 0.75 for sites installed inside electrical cabins or small buildings.

The proximity to buildings has also been also checked for the candidate stations. Following Abrahamson *et al.* (1991), we compute the minimum distance from the adjacent structures on the basis of the predominant vibration period of the structure, T_1. This latter is evaluated on the basis of the simplified evaluation proposed by NTC18 (Italian seismic code 2018):

$$T_1\,[\text{sec}] = C_1 * H^{3/4}, \tag{3}$$

where H is the building height and C_1 is an empirical coefficient, that varies from 0.05 to 0.085 depending on the construction material and structure type. On the basis of the empirical model proposed

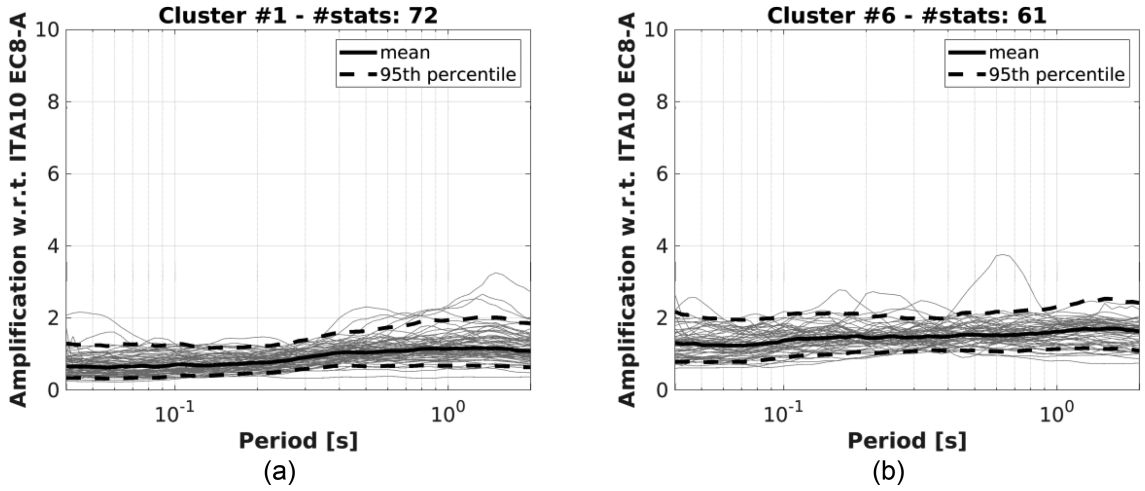

Figure 6. Amplification ($e^{\delta S2S}$) versus period. (a) cluster #1; (b) cluster #6.

Table 1. List of the proxies used to identify reference rock stations.

#	Proxy	Acceptance criterion
1	Housing (HOU)	Absent or limited interaction with structures (free-field condition)
2	Topographic condition (TOP)	Flat or smooth topographic surface
3	Surface geology (GEO)	Rock or stiff conditions from geological/lithological map
4	Average shear wave velocity in the first 30 m ($V_{S,30}$) measured or inferred from proxies	$V_{S,30} \geq 750$ m s^{-1}
5	Horizontal-to-vertical spectral ratio (H/V) of Fourier spectra of noise measurements (HVNSR) or coda-waves (HVSR-C) or *S* waves (HVSR-S) or acceleration response spectra (HVRS) of earthquake records	Flat or moderately broad-band curve
6	Site-to-Site term of the horizontal components ($\delta S2S$)	Negative or close to 0 on the entire period range

Table 2. Hierarchical index and weight values assigned to the proxies.

Proxy	Hierarchical index (HI)	Criterion		Proxy weight (PW)
HOU	0.5	Free-field condition		1
		Electrical transformation cabin		0.75
$V_{S,30}$	2	$\geq$1500 m s^{-1}		1
		$\geq$750 m s^{-1}		0.75
		$\geq$1500 m s^{-1} (inferred from topographic proxy)		0.5
		$\geq$750 m s^{-1} (inferred from topographic proxy)		0.375
GEO	2	EC8-A (scale-map $\geq$ 1:10,000)		1
		EC8-A (scale-map $<$ 1:10,000)		0.75
		EC8-B (scale-map $\geq$ 1:10,000)		0.5
		EC8-B (scale-map $<$ 1:10,000)		0.25
TOP	0.5	slope $\leq 15^\circ$		1
		$15^\circ <$ slope $\leq 30^\circ$		0.5
H/V	2	Flat (amplitude $< 2\sqrt{2}$)	HVNSR	1
			HVSR-C	1
			HVSR-S	0.5
			HVRS	0.5
		Broadband (amplitude $> 2\sqrt{2}$)	HVNSR	0.5
			HVSR-C	0.5
			HVSR-S	0.25
			HVRS	0.25
δS2S	1	cluster #1 within the confidence interval*		1
		cluster #1 beyond the confidence interval*		0.75
		cluster #6 within the confidence interval*		0.75
		cluster #6 beyond the confidence interval*		0.5

*5th–95th percentile.

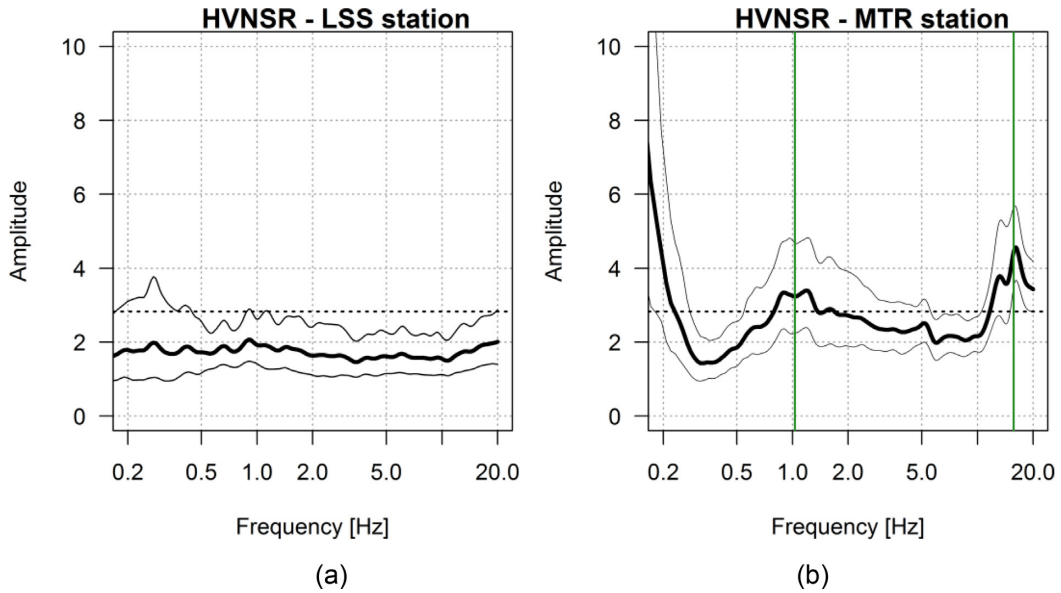

Figure 7. Horizontal-to-vertical spectral ratio analysis from noise measurements at (a) IT.LSS Leonessa and (b) IT.MTR-Montereale station and (from ITACA, Luzi *et al.* 2019).

by Abrahamson *et al.* (1991), a station may be considered in free-field condition when the distance from buildings with resonance frequency about 1 and 4 Hz is higher than 800 and 150 m, respectively (Stewart 2000). If the station meets this condition, PW = 1, otherwise PW = 0. Finally, we assign zero weight to recording stations installed in the vicinity of large dams (such as MSC station close to Campotosto dam in Abruzzo region).

Surface Geology—GEO

In order to evaluate the GEO proxy, the geological or lithological maps (available at different scales) are used to assign the EC8 soil categories to each station. The criterion is fully met when the station is installed on rock or other rock-like geological formation, according to the EC8-A ground type description, as inferred from geological maps at detailed scale. In our scheme, we also evaluate if stations are located on stiff soil, following the lithological description of the EC8-B category. Indeed, this kind of sites may be also characterized by flat or broad-band site response (Felicetta *et al.* 2018; Priolo *et al.* 2019).

Different weights (Table 2) are assigned: PW = 1 and 0.75 for EC8-A rock sites inferred from map with scale greater and smaller than 1:10 000, respectively; PW = 0.5 and 0.25 for EC8-B soil category inferred from map scale greater and lower than 1:10 000.

Topography—TOP

The TOP proxy is introduced to exclude sites with possible amplifications due to particular topographic settings (Paolucci 2002; Massa *et al.* 2014). To fully fulfill the acceptance criterion, the site must be located on either a flat surface or isolated slope and relief with average ground inclination from the horizontal plane less than 15°, following the prescriptions of some National building codes (AFPS95; NTC18). For station installed in very steep slopes (>30°), the weight is assumed to be zero.

Shear wave velocity—$V_{S,30}$

Due to the relation between shear wave velocity and stiffness of the material, the $V_{S,30}$ is the most common parameter used to recognize soils with similar site response (Borcherdt & Glassmoyer 1992). Similarly, to NEHRP site classification, we distinguish between hard and very hard rock sites, assigning different weights: if the shear wave velocity profile is measured by geophysical tests, at least in the uppermost 30 m, PW = 1 if $V_{S,30} > 1500\ \mathrm{m\,s^{-1}}$ and PW = 0.75 for $750\ \mathrm{m\,s^{-1}} < V_{S,30} \leq 1500\ \mathrm{m\,s^{-1}}$; if $V_{S,30}$ is inferred by proxies, such as surface geology or correlation with topographic slope, PW = 0.5 if $V_{S,30} > 1500\ \mathrm{m\,s^{-1}}$ and PW = 0.375 for $750\ \mathrm{m\,s^{-1}} < V_{S,30} \leq 1500\ \mathrm{m\,s^{-1}}$. In particular, when geophysical measurements are not available, the empirical correlation with slope by Wald & Allen (2007) is used to infer $V_{S,30}$. We select the value of $750\ \mathrm{m\,s^{-1}}$, as a lower limit, since in the investigated area the geological bedrock is often associated with soft rocks characterized by shear wave velocity in the range 700–800 $\mathrm{m\,s^{-1}}$ (Pacor *et al.* 2019).

Horizontal-to-vertical spectral ratio—H/V

The H/V represents a well-established technique to detect the fundamental resonance frequency of the site (f_0). H/V curves can be obtained from *in situ* noise measurements (HVNRS; Nakamura 1989; Bonnefoy-Claudet *et al.* 2008, and references listed therein) as well as from earthquake records. The latter can be used to produce H/V curves of Fourier amplitude spectra (HVSR; Lermo & Chávez-García 1993; Puglia *et al.* 2011) or damped elastic response spectra (HVRS; Puglia *et al.* 2011; Felicetta *et al.* 2018). After some test, the curves obtained from HVSR coda waves (HVSR-C) are generally similar to those calculated from noise measurements (HVNRS) as already observed in previous studies (Stehly *et al.* 2006). The mean H/V curves obtained from Fourier *S*-wave window (HVSR-S) are comparable to HVSR-C but the variability is generally higher, especially when directional effects are present or records from strong events at short epicentral distance are included (Puglia *et al.* 2011). Moreover, recent studies (e.g. Hassani *et al.* 2019) showed that in

Table 3. List of the cluster #1 stations with score (SUM_W) ≥ 4.75. For each station, the table reports: network code (NET CODE); station code (STA CODE); housing/proximity condition (HOU); housing weight (W_H); H/V analysis (HVtype); shape of H/V curve (H/V); weight for the H/V proxy (W_HV); shape of HVRS curve (HVRS); weight HVRS weight (W_HVRS); slope range (TOP); topographic weight (W_T); $V_{S,30}$ value (VS30); $V_{S,30}$ estimation method ($V_{S,30}$ type); $V_{S,30}$ weight (W_Vs); scale of the geological/lithological/litothecnical map; EC8 subsoil classification from surface geology (EC8); weight for the geological proxy (W_GEO); weight for cluster #1 (W_CL#1); number of available proxies (AV PROXIES). FF, free-field condition; CAB, electrical transformation cabin; NO-FF, no free-field condition; F, flat curve; BB, broad-band curve; P, picked curve.

NET CODE	STA CODE	HOU	W_HOU	HVtype	HV	W_HV	TOP	W_TOP	VS,30 [m/s]	VS,30 type	W_VS	GEO scale	EC8 geo	W_GEO	W_CL1	Available proxies	SUM_W
IT	BGR	FF	0.5	HVNSR	F	2	slope <=15°	0.5	829	Measured	1.5	5000	A	2	1	6	7.5
IT	LSS	FF	0.5	HVNSR	F	2	15°<slope<= 30°	0.25	1091	Measured	1.5	10000	A	2	1	6	7.25
IT	MVB	FF	0.5	HVNSR	F	2	slope <=15°	0.5	1046	Measured	1.5	5000	A	2	0.75	6	7.25
IT	GRN	CAB	0.375	HVNSR	F	2	15°<slope<= 30°	0.25	1015	Topographic proxy	0.75	5000	A	2	1	6	6.375
3A	MZ102	NO-FF	0	HVNSR	F	2	slope <=15°	0.5	837	Topographic proxy	0.75	5000	A	2	1	6	6.25
IV	ATVO	FF	0.5	HVNSR	F	2	slope <=15°	0.5	777	Topographic proxy	0.75	100000	A	1.5	1	6	6.25
IV	FIAM	FF	0.5	HVNSR	F	2	15°<slope<= 30°	0.25	1007	Topographic proxy	0.75	100000	A	1.5	1	6	6
IT	CSO1	FF	0.5	HVNSR	F	2	15°<slope<= 30°	0.25	1049	Topographic proxy	0.75	25000	A	1.5	0.75	6	5.75
IT	FMG	NO-FF	0	HVNSR	F	2	15°<slope<= 30°	0.25	790	Measured	1.5	5000	B	1	1	6	5.75
IT	SLO	FF	0.5	HVSR-C	BB	1	slope <=15°	0.5	823	Topographic proxy	0.75	10000	A	2	1	6	5.75
IV	SACS	FF	0.5	HVNSR	F	2	slope <=15°	0.5	364	Topographic proxy	0	100000	A	1.5	1	6	5.5
IV	CAFI	FF	0.5	HVNSR	F	2	slope <=15°	0.5	738	Topographic proxy	0	100000	A	1.5	1	6	5.5
IV	ATLO	FF	0.5	HVNSR	F	2	slope <=15°	0.5	511	Topographic proxy	0	100000	A	1.5	1	6	5.5
IV	POFI	FF	0.5	HVNSR	F	2	slope <=15°	0.5	443	Topographic proxy	0	100000	A	1.5	0.75	6	5.25
IT	MNF	NO-FF	0	HVNSR	F	2	15°<slope<= 30°	0.25	983	Topographic proxy	0.75	50000	A	1.5	0.75	6	5.25
IT	PAN	FF	0.5	HVSR-S	F	1	slope <=15°	0.5	870	Topographic proxy	0.75	20000	A	1.5	1	6	5.25
IT	PSC	FF	0.5	HVNSR	P	0	15°<slope<= 30°	0.25	1000	Measured	1.5	5000	A	2	1	6	5.25
IV	ATPI	FF	0.5	HVSR-S	F	1	slope <=15°	0.5	762	Topographic proxy	0.75	100000	A	1.5	1	6	5.25
IV	GUAR	FF	0.5	HVSR-S	F	1	slope <=15°	0.5	791	Topographic proxy	0.75	100000	A	1.5	1	6	5.25
IV	SACR		0	HVNSR	F	2	slope <=15°	0.5	501	Topographic proxy	0	100000	A	1.5	1	5	5
IV	SGTA		0	HVNSR	F	2	slope <=15°	0.5	701	Topographic proxy	0	100000	A	1.5	1	5	5
3A	MZ31	FF	0.5	HVNSR	F	2	slope <=15°	0.5	597	Topographic proxy	0	5000	B	1	1	6	5
IV	CIGN	FF	0.5	HVSR-S	F	1	slope <=15°	0.5	754	Topographic proxy	0.75	100000	A	1.5	0.75	6	5
IV	TRIV		0	HVNSR	F	2	slope <=15°	0.5	660	Topographic proxy	0	100000	A	1.5	0.75	5	4.75
IV	RM03		0	HVSR-C	F	2	slope <=15°	0.5	517	Topographic proxy	0	100000	A	1.5	0.75	5	4.75
IV	ATVA		0	HVSR-S	F	1	slope <=15°	0.5	800	Topographic proxy	0.75	100000	A	1.5	1	5	4.75
IT	ANT	NO-FF	0	HVNSR	P	0	slope <=15°	0.5	912	Measured	1.5	5000	A	2	0.75	6	4.75

Table 4. List of the cluster #6 stations with score (SUM_W) ≥ 4.75. See caption of Table 3.

NET CODE	STA CODE	HOU	W_HOU	HVtype	HV	W_HV	TOP	W_TOP	VS,30 [m/s]	VS,30 type	W_VS	GEO scale	EC8 geo	W_GEO	W_CL6	Available proxies	SUM_W
IT	ORC	NO-FF	0	HVSR-C	BB	1	slope <=15°	0.5	767	Measured	1.5	5000	A	2	0.75	6	5.75
IT	SNO	FF	0.5	HVNSR	F	2	slope <=15°	0.5	429	Topographic proxy	0	10000	A	2	0.75	6	5.75
IV	SNAL		0	HVNSR	F	2	slope <=15°	0.5	905	Topographic proxy	0.75	100000	A	1.5	0.75	5	5.5
IT	MMP1	FF	0.5	HVNSR	P	0	slope <=15°	0.5	800	Measured	1.5	5000	A	2	0.75	6	5.25
IT	SDM	CAB	0.375	HVNSR	F	2	slope <=15°	0.5	752	Measured	1.5	5000	C	0	0.75	6	5.125
IV	CAFR	FF	0.5	HVNSR	F	2	slope <=15°	0.5	602	Topographic proxy	0	100000	A	1.5	0.5	6	5
IT	CSC	NO-FF	0	HVNSR	F	2	15°<slope<= 30°	0.25	698	Measured	0	10000	A	2	0.75	6	5
IT	NRN	CAB	0.375	HVNSR	BB	1	slope <=15°	0.5	908	Topographic proxy	0.75	50000	A	1.5	0.75	6	4.875
IV	APEC	NO-FF	0	HVNSR	F	2	slope <=15°	0.5	683	Topographic proxy	0	100000	A	1.5	0.75	6	4.75

case of clear resonance frequencies, the outcomes from HVNRS and HVRS generally agree.

We define a ranking order based on the relevance of the different estimates: the preferred option is the HVNRS measurement; secondly, if HVNRS is not available, we consider Fourier spectra of coda waves of earthquake records (HVSR-C), or, if missing, the Fourier spectra of *S* waves (HVSR-S); the last option is the H/V computed on 5 per cent damped acceleration response spectra of earthquake recordings (HVRS).

In order to assign the weights to the H/V proxy, we define three possible shapes of the H/V curves: flat, broadband and peaked. In the first case (Fig. 7a), the H/V curve does not present any clear peak in the frequency band 0.2–20 Hz, range of potential engineering interest and amplitude does not exceed the threshold $2\sqrt{2}$ related to the vectorial sum of horizontal components (Puglia *et al.* 2011). In case of broad-band curve, the amplitude exceeds the threshold $2\sqrt{2}$ over a wide range of frequency. In the last case, the H/V curve presents at least one clear peak (green lines in Fig. 7b).

According to Table 2, different PWs are considered, combining the type of estimate (HVNRS, HVSR-C, HVSR-S and HVRS) and the H/V curve shape (flat or broadband).

Site-to-site term of horizontal component—$\delta S2S$

The site-to-site term may be considered as a proxy of the seismic response of the station (Al Atik *et al.* 2010), with the caveat that the amplification levels may be dependent on the reference sites adopted in the GMM calibration. The HI is set to 1 and the PW is assigned as a function of the cluster membership, attributing different values at clusters #1 and #6 and evaluating if the stations are or not within the confidence interval of each cluster (Table 2).

STATION SCORING

In order to constrain the reference rock sites identification to some geological and/or geophysical observations, we require that, at least,

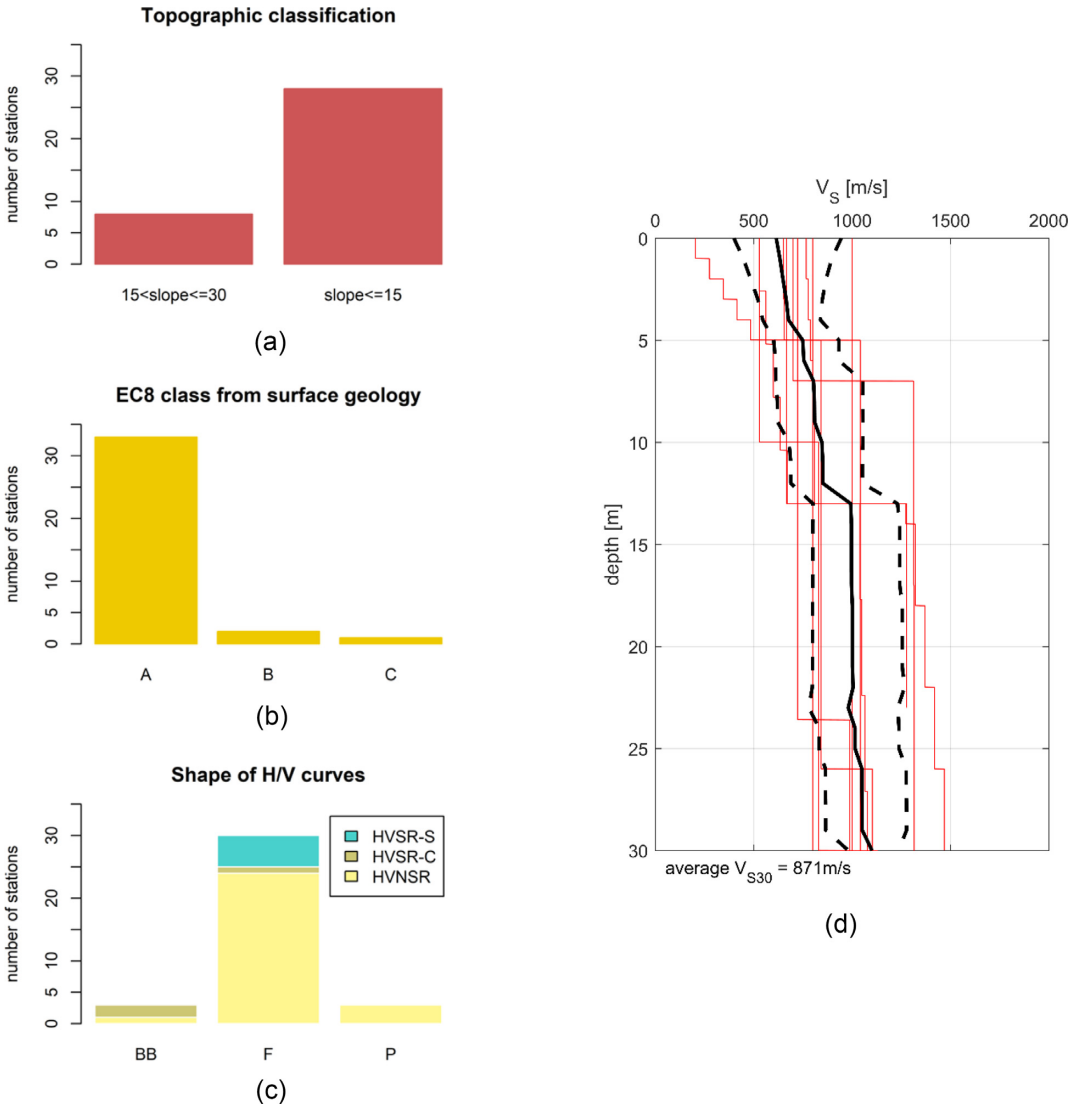

Figure 8. Distribution of the selected reference rock-sites in terms of: (a) slope range (TOP proxy); (b) EC8 class evaluated on surface geology (GEO proxy); (c) shape of H/V curves colored as function of the analysis type (HVNSR in yellow, HVSR-C in light brown, HVSR-S in teal) and (d) mean shear wave velocity profile (black line) and its standard deviation (dotted lines), up to 30 m, obtained from V_S profiles available for the selected reference rock-sites (grey lines). The average value of $V_{S,30}$ (871 m s^{-1}) is, also, reported.

Table 5. Percentage reduction between the predictions of EC8 for site A and Ref for the reference rock sites. The results of FEL18 are derived from Fig. 6 of the paper. The values of ΔY are averaged over 11 bins of distance [1–100 km] and 34 bins of magnitude [3.2–6.5].

	ΔY (per cent)				
	PGA	SA-T = 0.1 s	SA-T = 0.2 s	SA-T = 1 s	SA-T = 2 s
This study	40.5	46.7	36.7	4.2	6.9
FEL18	35.1	33.5	38.5	26.5	28.0

one of the three most important proxies (GEO, $V_{S,30}$ and H/V) is available. Then, we sum of the scores assigned at each proxy ($S = \sum^{H} I_i x P W_i$ where $i = 1 \ldots 6$) and assume that a station can be considered as a reference site if it reaches a minimum score of 4.75 out of 8 (Table 2). Adopting this threshold, almost 60 per cent of the required criteria are met. In order to give a statistical meaning to the choice of the threshold, we compute the statistical moments of the distribution of scores of all investigated stations: the median is 3.75, while the 84th percentile is 5.25. The adopted threshold (4.75) corresponds to the 75th percentile of the score distribution.

After the application of the weighting scheme, 27 stations out of 71 of cluster #1 and 9 out of 55 of cluster #6 can be considered as reference rock sites. No candidates reach the maximum awardable score (8) because the $V_{S,30}$ value greater than 1500 m s^{-1} is not represented in the Central Italy data set. The selected stations are listed in Tables 3 and 4 for cluster #1 and #6, respectively. Fig. 8 shows the distribution of the 36 reference rock-sites in terms topographic classification, EC8 class on surface geology, shape of Fourier H/V and HVRS curves. As expected, the majority of the candidates are located on rock with flat topography and the estimated H/V curves

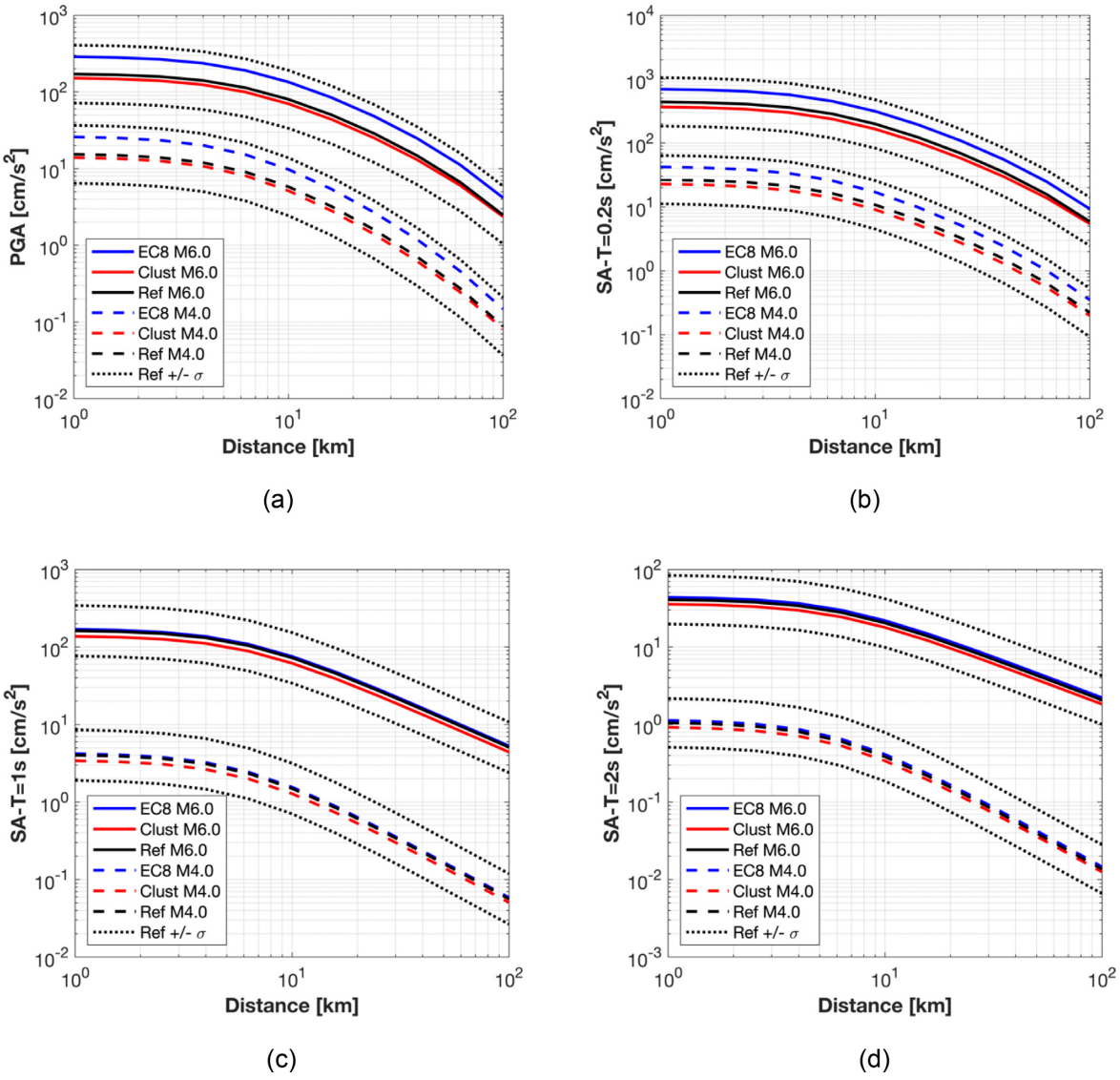

Figure 9. Predictions of EC8, Clust and Ref models for M 4.0 and M 6.0 as a function of Joyner-Boore distance: (a) PGA; (b) SA-T = 0.2 s; (c) SA-T = 1 s; (d) SA-T = 2 s. σ is the total standard deviation of the model Ref.

are flat; however, some exceptions are evident, such as IT.SDM (San Demetrio nei Vestini) station classified as EC8-C soil category from surface geology located on alluvial deposit of few metres.

The mean shear wave velocity up to 30 m of the candidate reference sites is $V_{S,30} = 871$ m s^{-1} obtained from 10 V_S profiles available (Fig. 8e).

The majority (about 70 per cent) of the stations of cluster #1 and #6 that do not reach the threshold value are characterized by a high frequency moderated peaked H/V curves and about half are classified in EC8-B and EC8-C site categories, according to the outcropping geology.

GROUND MOTION MODEL

Once the reference rock sites are identified, a set of GMMs is calibrated to test the impact of this selection. The functional form is:

$$\log_{10} Y = a + F_M(M) + F_R(M, R) + F_S + \delta B_e + \delta S2S_s + \varepsilon_{es}, \quad (4)$$

where the fixed-effects are the offset a, the magnitude term F_M, the distance term F_R and the site effect term F_S. The random-effects are performed on events (δB_e) and stations ($\delta S2S_s$) and ε_{es} is the aleatory error.

The magnitude term F_M is:

$$F_M(M) = \begin{cases} b_1 (M_w - M_h) & \text{for } M_w \le M_h \\ b_2 (M_w - M_h) & \text{otherwise} \end{cases}, \quad (5)$$

where b_1 and b_2 are coefficients obtained from the regression, M_h is the hinge magnitude. After some trial tests, the magnitude scaling is assumed to be a bi-linear function with a fixed hinge magnitude $M_h = 5.0$.

The distance term F_R is:

$$F_R(M, R) = [c_1 (M_w - M_{ref}) + c_2] \log_{10} \frac{\sqrt{R_{JB}^2 + h^2}}{R_{ref}} + c_3 \left(\sqrt{R_{JB}^2 + h^2} - R_{ref} \right), \quad (6)$$

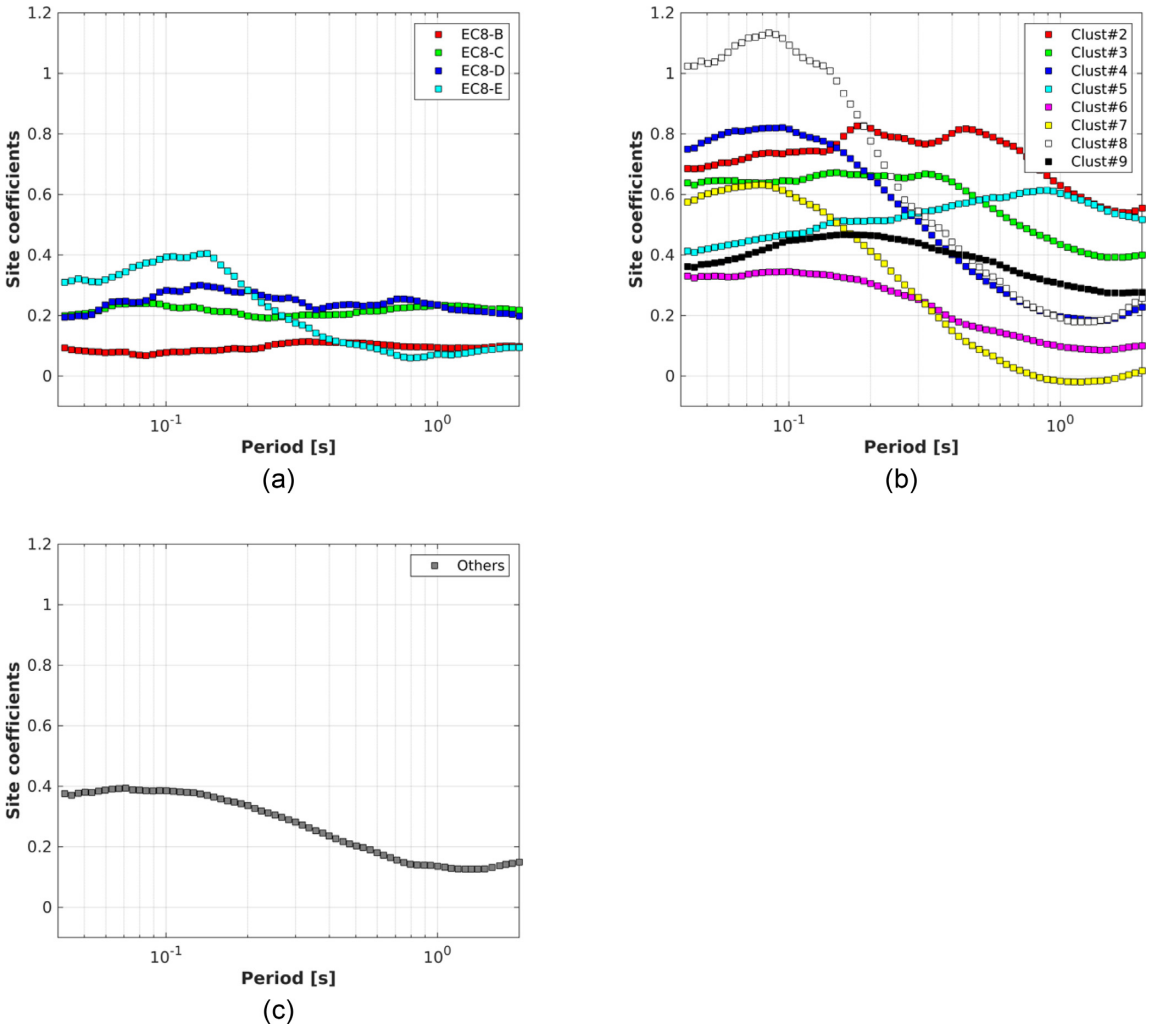

Figure 10. Site coefficients of model EC8 (a), Clust (b) and Ref (c).

where the c_1, c_2 and c_3 are obtained from the regression, M_{ref} is the reference magnitude, h is the pseudo-depth and R_{ref} is the reference distance ($R_{\text{ref}} = 1$ km). The model is calibrated for the Joyner–Boore distance, R_{JB}, and the maximum value is set to 120 km, since the bulk of data in concentrated in the distance range 10–100 km.

The site effect is introduced as $F_S = s_j C_j$, where s_j are the coefficients to be determined through the regression, while C_j are dummy variables used to denote the site categories. Three different definitions for the site categories, are considered:

1 *EC8*: Eurocode 8 site classification, where the coefficients of the site category EC8-A are set to zero ($s_{\text{EC8-A}} = 0$; $s_{\text{EC8-B}} \neq s_{\text{EC8-C}} \neq s_{\text{EC8-D}} \neq s_{\text{EC8-E}} \neq 0$).

2 *Clust*: Site classification after the cluster analysis, where the coefficients of the cluster #1 are set to zero ($s_{\#1} = 0$; $s_{\#2} \neq s_{\#3} \neq \ldots s_{\#9} \neq 0$).

3 *Ref*: Classification of the sites in two classes, (i) the reference rock sites, listed in Tables 4 and 5, and (ii) the remaining sites ('others') without any subdivisions (following Kotha *et al.* 2016); the coefficient of the reference rock site class is set to zero ($s_{\text{ref}} = 0$; $s_{\text{oth}} \neq 0$).

In a first stage of the analysis, we perform a nonlinear regression without the site term F_S to obtain the reference magnitude M_{ref}. After some trials, we fix $h = 6$ km, regardless the oscillation period, which corresponds to the averaged valued of the pseudo depth of the GMM proposed by Lanzano *et al.* (2019) for Italy. The coefficients a, b_1, b_2, c_1, c_2 and c_3, the site effect coefficients (fixed-effects) and the random-effects variabilities τ (between-event), ϕ_{S2S} (site-to-site) and ϕ_0 (event- and site-corrected residuals) are derived by the calibration of a linear ordinary least-squares mixed-effect model. The calibration results of the three models for the geometric mean of horizontal components of PGA and 69 ordinates of the acceleration spectra SA (5 per cent damping), in the period range $T = 0.04$–2 s, are reported in the ESUPP1.

Fig. 9 illustrates the plot of the attenuation with distance at two magnitudes (4.0 and 6.0) of the three models (EC8, Clust and Ref), considering the predictions for the site class set to zero in each model (reference level). As expected, the predictions at short periods (PGA in Fig. 9a and $T = 0.2$ s in Fig. 9b) for the reference sites of Ref and Clust are remarkably lower than those obtained for EC8 and the reduction is almost independent on distance.

The trend of coefficients for the three models is shown in Fig. 10. Only the Clust model (Fig. 10b) allow to clearly distinguish the seismic response among site-categories, resembling the amplification functions, showed in Fig. 5.

The between-event variability τ and the residual aleatory variability ϕ_0 are unaffected by the classification scheme adopted for

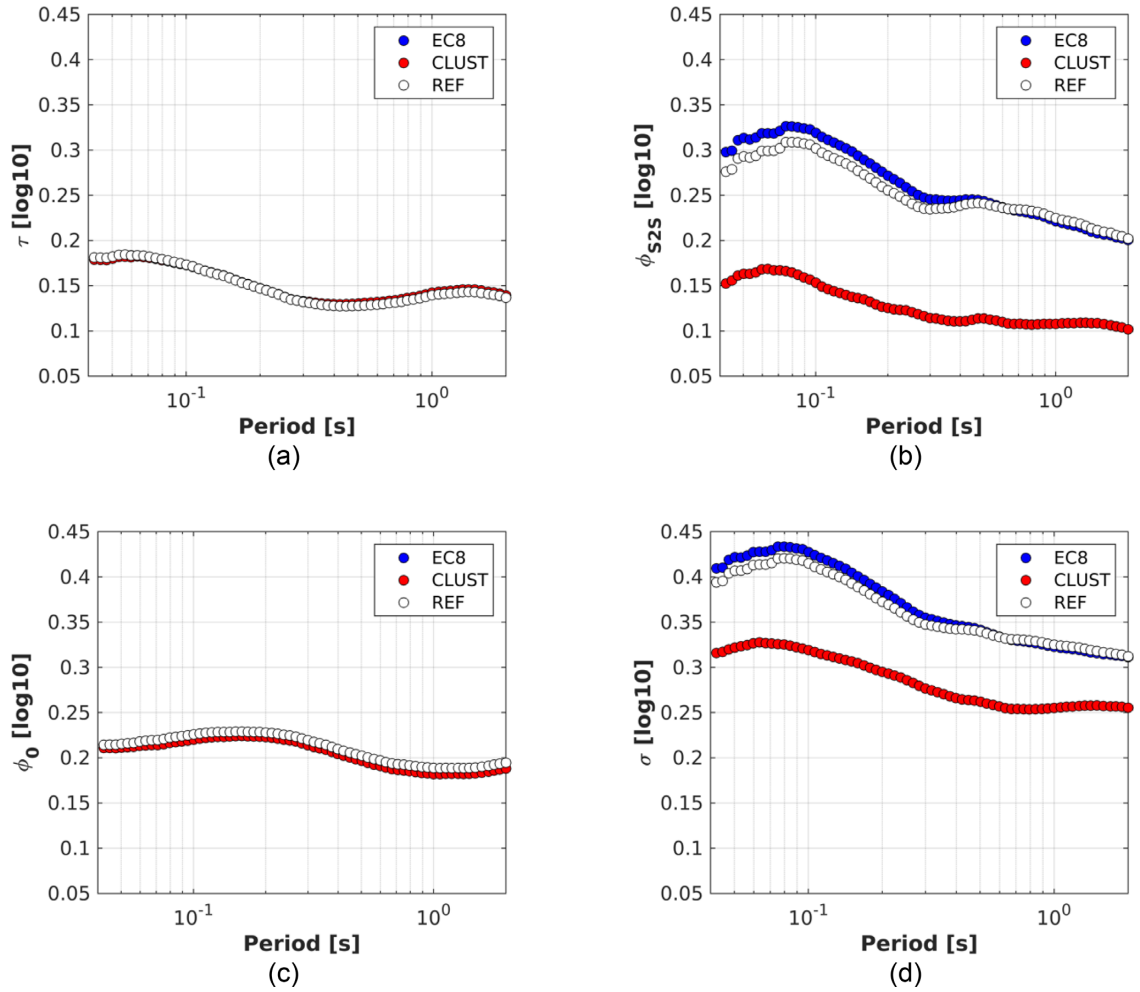

Figure 11. Standard deviations of EC8, Clust and Ref models: (a) between-event term; (b) site-to-site term; (c) variability of the event- and site-corrected residuals and (d) total sigma.

calibrating the GMMs (Figs 11a and c). The site-to-site variability ϕ_{S2S} of Clust model is, instead, significantly lower than those found for EC8 and Ref models (Fig. 11b). This is not surprising since the Clust model is a data-driven approach that, however, cannot be adopted for other data set without the introduction of any explanatory variable related to the sites (Kotha *et al.* 2018).

As a matter of fact, most of the stations in Central Italy are classified as EC8-B class on the basis of surface geology (Fig. 3). However, the assignment of the site classes of the EC8 according to geological proxies is too approximate, especially if inferred from small-scale maps (e.g. 1:50 000). Recent studies (Felicetta *et al.* 2018; Forte *et al.* 2019) showed that, within the same geological unit, the V_S profiles and the corresponding $V_{S,30}$, may be very different.

DISCUSSIONS AND CONCLUSIONS

The main objective of this work is to improve the strategy formulated by FEL18 to identify seismic stations that can be considered as reference rock sites, increasing the set of proxies for the site responses and introducing a scoring scheme. The decision matrix method (DDM) is used to rank the candidate stations, allowing to perform the selection including several elements (e.g. geology, installation feature, $V_{S,30}$ values) that could influence the site response. DDM is suitable for such analysis since some of these proxies are not measurable (such as the geological map) and cannot be easily combined with the others. The DMM procedure also allows us to effectively weight the relevance of the considered factors.

To expand the number of parameters, useful for site characterization, in addition to the geophysical measurements and the geological data, we also exploited the results from the analysis of the seismic records. At the end, we individuated six proxies: four are related to the analysis of geophysical and seismological data (the site term from residual analysis, the resonance frequencies from H/Vs, the average shear wave velocity in the first 30 m); the remaining ones concern geomorphological and installation features (outcropping rocks or stiff soils, flat topography and absence of interaction with structures). The proposed proxies are designed to be consistent with the data and metadata provided by qualified ground motion databases, from which the site information can be easily retrieved and the seismological analyses performed. We allow for the partial overlap among proxies, preserving the peculiarity of each criterion: for example, $\delta S2S$ and H/V are representative of similar information, but H/V also considers the vertical motion, while $\delta S2S$ only refers to the horizontal component. Another example is the topographic slope that contributes both to the TOPO proxy and to inferred $V_{S,30}$.

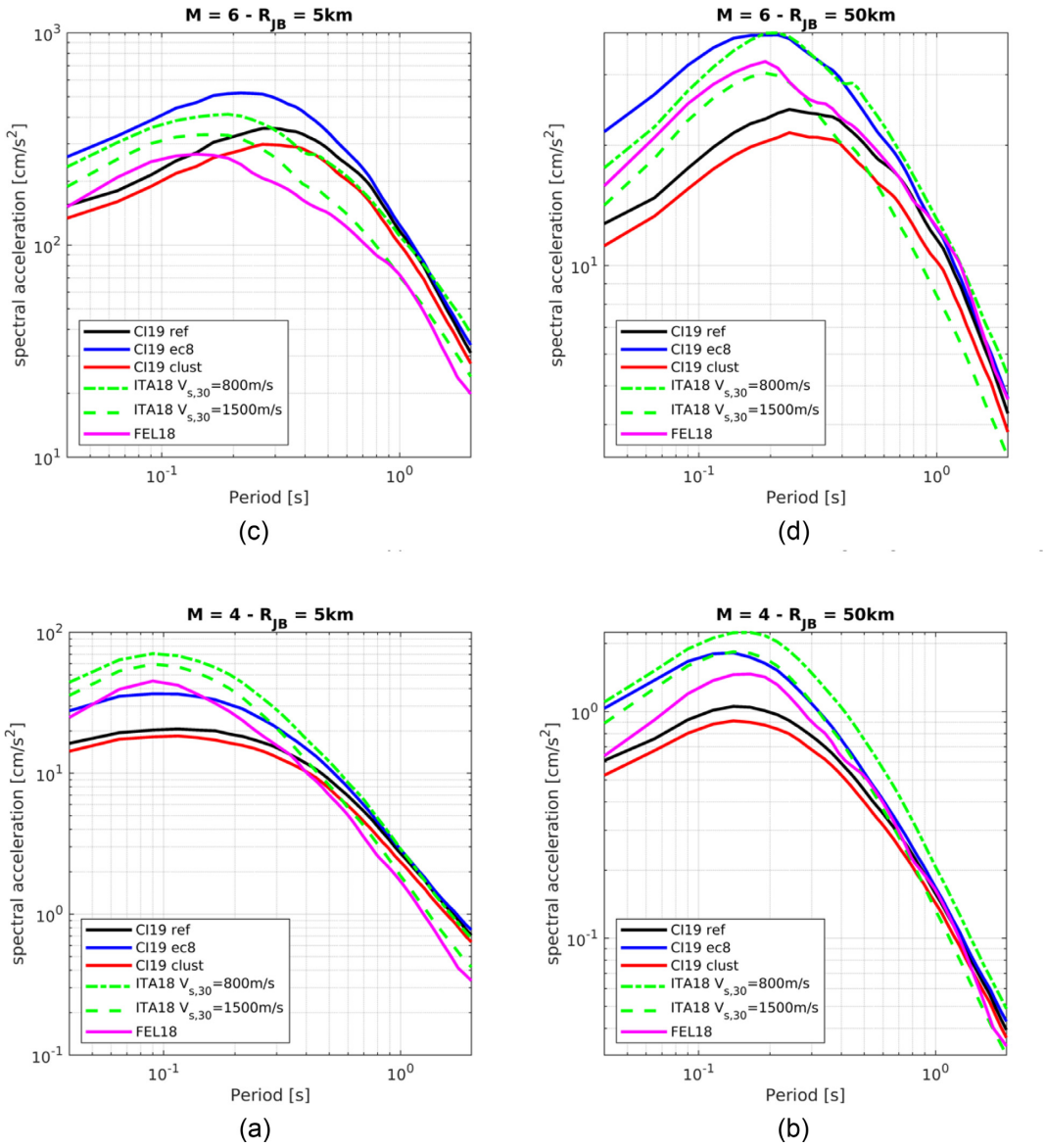

Figure 12. Acceleration response spectra (5 per cent damping) predicted by the models EC8, Clust and Ref. The GMMs ITA18 (Lanzano *et al.* 2019) and FEL18 (Felicetta *et al.* 2018) are added for comparison.

Because of the different capability of the selected proxies to represent the seismic response of the stations, we introduced a hierarchical index, variable from 0.5 to 2, aimed at ranking these parameters. We assumed that the most important parameters for site-effect characterization are the surface geology, the $V_{S,30}$ and the H/V from noise measurement, while topography and housing are considered less relevant than others in the reference site identifications. In particular, the surface geology is available at detailed scales in several Italian regions, especially after the seismic microzonation studies and the activity of site characterization of the seismic stations promoted throughout Italy in the last ten years.

We give a lower HI to TOPO (also used in the $V_{S,30}$ estimates) and to the influence of housing/proximity (HOU), also recognizable by H/V, precisely because of the partial overlap with other proxies. The fulfillment of the criteria relative to the first three site parameters allows to select potential reference-rock sites and may be very useful during the design phase of seismic networks.

Furthermore, we proposed a weighting scheme for each proxy, variable from 0 to 1, to take into account the presence (or absence) and the quality of the information. Finally, by the combination of the weights and the indexes, we assigned an overall score and identified the reference sites as those that exceed a given threshold. This scoring scheme allows somehow to account for the epistemic uncertainty associated to the selected proxies and to qualify the confidence we associate to the identified reference rock sites.

The application of this procedure is carried out on a large data set of seismic records collected in Central Italy. This data set, composed by more than 30 000 waveforms, includes more than 450 recording sites and more than 450 earthquakes in the magnitude range (M_L) 3.2–6.5. We ranked the Central Italy stations using the scoring scheme of Table 2, using a threshold value of 4.75. A total of 36 out of 133 candidate stations were identified as reference sites. The majority of these stations are installed on rock, with flat topography, but this is not sufficient to guarantee the absence of amplifications, especially at high frequencies. This result highlights the importance

to integrate geomorphological information with the outcomes of the seismological analyses to exclude the stations affected by resonance phenomena.

The impact of the introduction of reference sites into GMM calibration is evaluated in Table 5, by means of the normalized difference between the median predictions of the EC-8 and Ref models.

The high-frequency median ground motion for the reference rock sites is significantly lower w.r.t. the EC8-A sites, with reductions of up to 44 per cent at $T = 0.1$ s. These results are quite similar to the findings of FEL18, except for long periods, where we have a smaller drop (at $T = 1$ s 4.2 per cent versuss 26.5 per cent). On the other hand, the standard deviations of the EC8 and Ref models do not change, since they have very similar site-to-site variability. The latter is reduced only in case of Clust model, where the site classification is data-driven. Further efforts should be spent to investigate the best proxies to predict the ground motion for each cluster (Kotha *et al.* 2018).

Fig. 12 shows the spectra predicted at different scenarios for the reference conditions of each model. In addition, the FEL18 and the recent GMMs for Italy (named ITA18) are added to the plot, considering $V_{S,30} = 800$ m s^{-1} and $V_{S,30} = 1500$ m s^{-1}. The spectra of the models calibrated in Central Italy reflect the rich low frequency energy content ($T > 0.5$ s) of the records of the events in such small area, as already observed in other studies (Lanzano *et al.* 2016; Bindi *et al.* 2019): the Ref predictions seem to be captured by ITA18 at $V_{S,30} = 800$ m s^{-1} at low frequencies; while, at high frequency, the Ref values are even lower than ITA18 at $V_{S,30} = 1500$ m s^{-1}.

The last evidence suggests that the assessment of the seismic motion level for the reference sites cannot be trivially a scaling of another model to a value of $V_{S,30}$ sufficiently low. On the contrary, additional site parameters must be introduced and analysed to select and rank the candidate reference sites and an *ad hoc* model or corrective terms must be calibrated.

In the end, the use of different proxies is promising in the identification of the reference rock site. The proposed model can be considered valid for Central Italy (region-specific) and the proposed methodology should be implemented and validated in other regions, characterized by different tectonic settings and geomorphological environments.

ACKNOWLEDGEMENTS

The work presented in this paper was partially by the SIGMA2 consortium (EDF, CEA, PG&E, SwissNuclear, Orano, CEZ, CRIEPI) 2017–2021 (http://www.sigma-2.net/; accessed October 2019). The authors also wish to thank John Douglas and Alain Pecker for the useful suggestions that improved the quality of the work.

The results of this work were also used in the Project MIUR-FISR (Fondo Integrativo Speciale per la Ricerca) 2016 ‘Systematic source-, site- and path-effects on ground motion variability: the case study of Central Italy’, coordinated by Maria D’Amico and funded by the Istituto Nazionale di Geofisica e Vulcanologia (INGV).

The Authors wish to thank Olga-Joan Ktenidou and the other anonymous reviewer that provided useful and interesting comments that helped us in the review of the manuscript.

REFERENCE

Abrahamson, N.A., Schneider, J.F. & Stepp, J.C., 1991. Empirical spatial coherency functions for application to soil-structure interaction analyses, *Earthq. Spectra,* **7**(1), 1–27.

AFPS95, 1995. Recommandations pour la redaction de regles relatives aux ouvrages dans les regions sujettes aux seismes.

Anderson, J.G. & Hough, S.E., 1984. A model for the shape of the Fourier amplitude spectrum of acceleration at high frequencies, *Bull. seism. Soc. Am.,* **74**(5), 1969–1993.

Al Atik, L., Abrahamson, N., Bommer, J.J., Scherbaum, F., Cotton, F. & Kuehn, N., 2010. The variability of ground-motion prediction models and its components, *Seismol. Res. Lett.,* **81**(5), 794–801.

Bindi, D., Pacor, F., Luzi, L., Massa, M. & Ameri, G., 2009. The Mw 6.3, 2009 L’Aquila earthquake: source, path and site effects from spectral analysis of strong motion data, *Geophys. J. Int.,* **179**(3), 1573–1579.

Bindi, D., Pacor, F., Luzi, L., Puglia, R., Massa, M., Ameri, G. & Paolucci, R., 2011. Ground motion prediction equations derived from the Italian strong motion database, *Bull. Earthq. Eng.,* **9**(6), 1899–1920.

Bindi, D., Picozzi, M., Spallarossa, D., Cotton, F. & Kotha, S.R., 2019. Impact of magnitude selection on aleatory variability associated with ground-motion prediction equations. Part II—analysis of the between-event distribution in Central Italy, *Bull. seism. Soc. Am.,* **109**(1), 251–262.

Boncio, P., Lavecchia, G. & Pace, B., 2004. Defining a model of 3D seismogenic sources for Seismic Hazard Assessment applications: the case of Central Apennines (Italy), *J. Seismol.,* **8**(3), 407–425.

Bonnefoy-Claudet, S., Köhler, A., Cornou, C., Wathelet, M. & Bard, P.Y., 2008. Effects of love waves on microtremor H/V ratio, *Bull. seism. Soc. Am.,* **98**(1), 288–300.

Borcherdt, R.D. & Glassmoyer, G., 1992. On the characteristics of local geology and their influence on ground motions generated by the Loma Prieta earthquake in the San Francisco Bay region, California, *Bull. seism. Soc. Am.,* **82,** 603–641.

Bordoni, P. *et al.*, 2017. Le attività per la caratterizzazione dei siti della rete sismica nazionale dell’INGV. 36° Convegno GNGTS, Trieste 14 – 16 November 2017 (in Italian).

Boore, D.M., Stewart, J.P., Seyhan, E. & Atkinson, G.M., 2014. NGA-West 2 equations for predicting PGA, PGV, and 5%-damped PSA for shallow crustal earthquakes, *Earthq. Spectra,* **30**(3), 1057–1085.

BSSC(2003). NEHRP Recommended Provisions for Seismic Regulations for New Buildings and Other Structures (Fema 450).

Burjanek, J., Edwards, B. & Fah, D., 2014. Empirical evidence of local seismic effects at sites with pronounced topography: a systematic approach, *Geophys. J. Int.,* **197**(1), 608–619.

Cadet, H., Bard, P. Y. & Rodriguez-Marek, A., 2010. Defining a standard rock site: propositions based on the KiK-net database, *Bull. seism. Soc. Am.,* **100**(1), 172–195.

CEN (Comité Europé en de Normalisation), 2004. Eurocode 8: design of structures for earthquake resistance-Part 1: general rules, seismic actions and rules for buildings, Comité Européen de Normalisation Brussels; May; ⟨ http://www.cen.eu/cenorm/homepage.htm⟩.

Chiaraluce, L. *et al.*, 2017. The 2016 Central Italy seismic sequence: a first look at the mainshocks, aftershocks, and source models, *Seismol. Res. Lett.,* **88**(3), 757–771.

Cultrera, G., Di Giulio, G., Cornou, C., Bard, P.Y. & Al Tfaily, B., 2019. Best practice and quality assessment procedures for site characterization at seismic station: an European initiative, in *Proceedings of the AGU 2019 Fall Meeting,* 09–13 December 2019, San Francisco, CA, USA.

David, A. & Vassilvitskii, S. 2007. K-means++: the advantages of careful seeding, in *SODA ‘07: Proceedings of the Eighteenth Annual ACM-SIAM Symposium on Discrete Algorithms,* pp. 1027–1035.

Di Naccio, D. *et al.*, 2017. Seismic amplification in a fractured rock site. The case study of San Gregorio (L’Aquila, Italy), *Phys. Chem. Earth, Parts A/B/C,* **98,** 90–106.

Ditommaso, R., Mucciarelli, M., Gallipoli, M.R. & Ponzo, F.C., 2010. Effect of a single vibrating building on free-field ground motion: numerical and experimental evidences, *Bull. Earthq. Eng.,* **8,** 693–703.

Felicetta, C., Lanzano, G., D’Amico, M., Puglia, R., Luzi, L. & Pacor, F., 2018. Ground motion model for reference rock sites in Italy, *Soil Dyn. Earthq. Eng.,* **110,** 276–283.

Ferrarini, F., Lavecchia, G., de Nardis, R. & Brozzetti, F., 2015. Fault geometry and active stress from earthquakes and field geology data analysis:

the Colfiorito 1997 and L'Aquila 2009 Cases (Central Italy). *Pure appl. Geophys.,* **172**(5), 1079–1103.

Forte, G., Chioccarelli, E., De Falco, M., Cito, P., Santo, A. & Iervolino, I., 2019. Seismic soil classification of Italy based on surface geology and shear-wave velocity measurements, *Soil Dyn. Earthq. Eng.,* **122,** 79–93.

Gallipoli, M.R., Mucciarelli, M., Castro, R.R., Monachesi, G. & Contri, P., 2004. Structure, soil-structure response and effects of damage based on observations of horizontal-to-vertical spectral ratios of microtremors, *Soil Dyn. Earthq. Eng.,* **24**(6), 487–495.

Gorini, A. *et al.*, 2010. The Italian strong motion network, *Bull. Earthq. Eng.,* **8**(5), 1075–1090.

Hassani, B., Yong, A., Atkinson, G. M., Feng, T. & Meng, L., 2019. Comparison of site dominant frequency from earthquake and microseismic data in California, *Bull. seism. Soc. Am.,* **109**(3), 1034–1040.

Kotha, S.R., Bindi, D. & Cotton, F., 2016. Partially non-ergodic region specific GMPE for Europe and Middle-East, *Bull. Earthq. Eng.,* **14**(4), 1245–1263.

Kotha, S.R., Cotton, F. & Bindi, D., 2018. A new approach to site classification: mixed-effects ground motion prediction equation with spectral clustering of site amplification functions, *Soil Dyn. Earthq. Eng.,* **110,** 318–329.

Ktenidou, O.J. & Abrahamson, N., 2016. Empirical estimation of high-frequency ground motion on hard rock, *Seismol. Res. Lett.,* **87,** 1465–1478.

Lanzano, G., Luzi, L., Pacor, F., Puglia, R., D'Amico, M., Felicetta, C. & Russo, E., 2016. Preliminary analysis of the accelerometric recordings of the August 24th, 2016 M_W 6.0 Amatrice earthquake, *Ann. Geophys.,* **59**.

Lanzano, G., D'Amico, M., Felicetta, C., Luzi, L. & Puglia, R., 2017. Update of the single-station sigma analysis for the Italian strong-motion stations, *Bull. Earthq. Eng.,* **15**(6), 2411–2428.

Lanzano, G., Luzi, L., Pacor, F., Felicetta, C., Puglia, R., Sgobba, S. & D'Amico, M., 2019. A revised ground motion prediction model for shallow crustal earthquakes in Italy, *Bull. seism. Soc. Am.,* **109**(2), 525–540.

Lermo, J. & Chávez-García, F.J., 1993. Site effect evaluation using spectral ratios with only one station, *Bull. seism. Soc. Am.,* **83,** 1574–1594.

Luzi, L., Bindi, D., Puglia, R., Pacor, F. & Oth, A. 2014. Single station sigma for Italian strong-motion stations, *Bull. seism. Soc. Am.,* **104**(1), 467–483.

Luzi, L., Pacor, F. & Puglia, R., 2019. Italian Accelerometric Archive v3.0. Istituto Nazionale di Geofisica e Vulcanologia, Dipartimento della Protezione Civile Nazionale. doi:10.13127/itaca.3.0.

Marzorati, S., Ladina, C., Falcucci, E., Gori, S., Saroli, M., Ameri, G. & Galadini, F., 2011. Site effects "on the rock": the case of Castelvecchio Subequo (L'Aquila, central Italy), *Bull. Earthq. Eng.,* **9,** 841–868.

Massa, M., Barani, S. & Lovati, S., 2014. Overview of topographic effects based on experimental observations: meaning, causes and possible interpretations, *Geophys. J. Int.,* **197**(3), 1537–1550.

Nakamura, Y, 1989. A method for dynamic characteristics estimation of subsurface using microtremor on the ground surface. *QR Railw Tech. Res. Inst*., **30,** 25–33.

NTC18, 2018. Norme Tecniche per le Costruzioni (NTC18). Decreto Ministero Infrastrutture. GU Serie Generale n. 42 del 20-02-2018 – Suppl. Ordinario n. 8 (in Italian).

Pacor, F. *et al.*, 2011. Overview of the Italian strong motion database ITACA 1.0, *Bull. Earthq. Eng.,* **9**(6), 1723–1739.

Pacor, F. *et al.*, 2019. Amplification functions in the epicentral area of the 2016, Mw 6.0, Amatrice earthquake (Central Italy) using ground-motion records and geological-geophysical data, in *Proceedings of 7th International Conference on Earthquake Geotechnical Engineering,* Rome, Italy, 17–20 June.

Pagliaroli, A. *et al.*, 2019. Site response analyses for complex geological and morphological conditions: relevant case-histories from 3rd level seismic microzonation in Central Italy, *Bull. Earthq. Eng.,* doi:10.1007/s10518-019-00610-7.

Paolucci, R., 2002. Amplification of earthquake ground motion by steep topographic irregularities, *Earthq. Eng. Struct. Dyn.,* **31,** 1831–1853.

Pergalani, F. *et al.*, 2019. Seismic microzoning map: approaches, results and applications after the 2016–2017 Central Italy seismic sequence, *Bull. Earthq. Eng.,* doi:10.1007/s10518-019-00640-1.

Pischiutta, M., Rovelli, A., Vannoli, P. & Calderoni, G., 2011. Recurrence of horizontal amplification at rock sites: a test using H/V based ground motion prediction equations,in *Proceedings of the 4th IASPEI/IAEE International Symposium,* Santa Barbara, CA, August 23–26.

Pondrelli, S., Salimbeni, S. & Perfetti, P., 2016. Moment tensor solutions for the Amatrice 2016 seismic sequence, *Annals Geoph*., **59,** 1–6.

Porreca, M. *et al.*, 2018. Seismic reflection pro filesand subsurface geology of the area interested by the 2016–2017 earthquake sequence (Central Italy), *Tectonics,* **37,** 1116–1137.

Priolo, E. *et al.*, 2019. Seismological analyses for the seismic microzonation of the 138 municipalities damaged by the 2016–2017 seismic sequence in Central Italy,*Bull. Earthq. Eng.,* https://doi.org/10.1007/s10518-019-00652-x.

Pugh, S., 1981. Concept selection: a method that works, in *Review of Design Methodology. Proceedings of International Conference on Engineering Design, March 1981,* ed. Hubka, V., Heurista, pp. 497–506.

Puglia, R., Albarello, D., Gorini, A., Luzi, L., Marcucci, S. & Pacor, F., 2011. Extensive characterization of Italian accelerometric stations from single-station ambient-vibration measurements, *Bull. Earthq. Eng.,* **9,** 1821–1838.

Puglia, R. *et al.*, 2015. On the performances of site parameters for soil classification, in *Engineering Geology for Society and Territory,* Vol. **5,** eds Lollino, G., Manconi, A., Guzzetti, F., Culshaw, M., Bobrowsky, P. & Luino, F., Springer.

Rodriguez-Marek, A., Rathje, E. M., Bommer, J. J., Scherbaum, F. & Stafford, P.J., 2014. Application of single-station sigma and site-response characterization in a probabilistic seismic-hazard analysis for a new nuclear site, *Bull. seism. Soc. Am.,* **104**(4), 1601–1619.

Rovelli, A., Caserta, A., Marra, F. & Ruggiero, V., 2002. Can seismic waves be trapped inside an inactive fault zone? The case study of Nocera Umbra, Central Italy, *Bull. seism. Soc. Am.,* **92**(6), 2217–2232.

Stewart, J.P., 2000. Variations between foundation-level and free-field earthquake ground motions. *Earthq. Spectra,* **16**(2), 511–532.

Stewart, P., Fenves, L. & Seed, B., 1999. Seismic soil-structure interaction in buildings. I: analytical methods, *J. Geotech. Geoenviron. Eng.,* **125**(1), 26–37.

Steidl, H.J., Tumarkin, A.G. & Archuleta, R.J., 1996. What is a reference site? *Bull. seism. Soc. Am.,* **86**(6), 1733–1748.

Stehly, L., Campillo, M. & Shapiro, N.M., 2006. A study of the seismic noise from its long-range correlation properties, *J. geophys. Res.,* **111,** 1–12.

Wald, D.J. & Allen, T.I., 2007. Topographic slope as a proxy for seismic site conditions and amplification, *Bull. seism. Soc. Am.,* **97**(5), 1379–1395.

SUPPLEMENTARY INFORMATION

Supplementary data are available at *GJI* online.

Ground Motion Models (GMMs) Coefficients of the EC8, Clust and Ref model

Table S1. Coefficients and standard deviations of the Ref model.
Table S2. Coefficients and standard deviations of the Clust model.
Table S3. Coefficients and standard deviations of the EC8 model.

Please note: Oxford University Press is not responsible for the content or functionality of any supporting materials supplied by the authors. Any queries (other than missing material) should be directed to the corresponding author for the paper.

Key words

Authors are requested to choose key words from the list below to describe their work. The key words will be printed underneath the summary and are useful for readers and researchers. Key words should be separated by a semi-colon and listed in the order that they appear in this list. An article should contain no more than six key words.

COMPOSITION and PHYSICAL PROPERTIES
Composition and structure of the continental crust
Composition and structure of the core
Composition and structure of the mantle
Composition and structure of the oceanic crust
Composition of the planets
Creep and deformation
Defects
Elasticity and anelasticity
Electrical properties
Equations of state
Fault zone rheology
Fracture and flow
Friction
High-pressure behaviour
Magnetic properties
Microstructure
Permeability and porosity
Phase transitions
Plasticity, diffusion, and creep

GENERAL SUBJECTS
Core
Gas and hydrate systems
Geomechanics
Geomorphology
Glaciology
Heat flow
Hydrogeophysics
Hydrology
Hydrothermal systems
Infrasound
Instrumental noise
Ionosphere/atmosphere interactions
Ionosphere/magnetosphere interactions
Mantle processes
Ocean drilling
Structure of the Earth
Thermochronology
Tsunamis
Ultra-high pressure metamorphism
Ultra-high temperature metamorphism

GEODESY and GRAVITY
Acoustic-gravity waves
Earth rotation variations
Geodetic instrumentation
Geopotential theory
Global change from geodesy
Gravity anomalies and Earth structure
Loading of the Earth
Lunar and planetary geodesy and gravity
Plate motions
Radar interferometry
Reference systems
Satellite geodesy
Satellite gravity
Sea level change
Seismic cycle
Space geodetic surveys
Tides and planetary waves
Time variable gravity
Transient deformation

GEOGRAPHIC LOCATION
Africa
Antarctica
Arctic region
Asia
Atlantic Ocean
Australia
Europe
Indian Ocean
Japan
New Zealand
North America
Pacific Ocean
South America

GEOMAGNETISM and ELECTROMAGNETISM
Archaeomagnetism
Biogenic magnetic minerals
Controlled source electromagnetics (CSEM)
Dynamo: theories and simulations
Electrical anisotropy
Electrical resistivity tomography (ERT)
Electromagnetic theory
Environmental magnetism
Geomagnetic excursions
Geomagnetic induction
Ground penetrating radar
Magnetic anomalies: modelling and interpretation
Magnetic fabrics and anisotropy
Magnetic field variations through time
Magnetic mineralogy and petrology
Magnetostratigraphy
Magnetotellurics
Marine electromagnetics
Marine magnetics and palaeomagnetics
Non-linear electromagnetics
Palaeointensity
Palaeomagnetic secular variation
Palaeomagnetism
Rapid time variations
Remagnetization
Reversals: process, time scale, magnetostratigraphy
Rock and mineral magnetism
Satellite magnetics

GEOPHYSICAL METHODS
Downhole methods
Fourier analysis
Fractals and multifractals
Image processing
Instability analysis
Interferometry
Inverse theory
Joint inversion
Neural networks, fuzzy logic
Non-linear differential equations
Numerical approximations and analysis
Numerical modelling
Numerical solutions
Persistence, memory, correlations, clustering
Probabilistic forecasting
Probability distributions
Self-organization
Spatial analysis
Statistical methods
Thermobarometry
Time-series analysis
Tomography
Waveform inversion
Wavelet transform

PLANETS
Planetary interiors
Planetary volcanism

SEISMOLOGY
Acoustic properties
Body waves
Coda waves
Computational seismology
Controlled source seismology
Crustal imaging
Earthquake dynamics
Earthquake early warning
Earthquake ground motions
Earthquake hazards
Earthquake interaction, forecasting, and prediction
Earthquake monitoring and test-ban treaty verification
Earthquake source observations
Guided waves
Induced seismicity
Interface waves
Palaeoseismology
Rheology and friction of fault zones
Rotational seismology
Seismic anisotropy
Seismic attenuation
Seismic instruments
Seismic interferometry
Seismicity and tectonics
Seismic noise
Seismic tomography
Site effects
Statistical seismology
Surface waves and free oscillations
Theoretical seismology

Tsunami warning
Volcano seismology
Wave propagation
Wave scattering and diffraction

TECTONOPHYSICS
Backarc basin processes
Continental margins: convergent
Continental margins: divergent
Continental margins: transform
Continental neotectonics
Continental tectonics: compressional
Continental tectonics: extensional
Continental tectonics: strike-slip and transform
Cratons
Crustal structure
Diapirism
Dynamics: convection currents, and mantle plumes
Dynamics: gravity and tectonics
Dynamics: seismotectonics
Dynamics and mechanics of faulting
Dynamics of lithosphere and mantle
Folds and folding
Fractures, faults, and high strain deformation zones
Heat generation and transport
Hotspots
Impact phenomena
Intra-plate processes
Kinematics of crustal and mantle deformation
Large igneous provinces
Lithospheric flexure
Mechanics, theory, and modelling
Microstructures
Mid-ocean ridge processes
Neotectonics
Obduction tectonics
Oceanic hotspots and intraplate volcanism
Oceanic plateaus and microcontinents
Oceanic transform and fracture zone processes
Paleoseismology
Planetary tectonics
Rheology: crust and lithosphere
Rheology: mantle
Rheology and friction of fault zones
Sedimentary basin processes
Subduction zone processes
Submarine landslides
Submarine tectonics and volcanism
Tectonics and climatic interactions
Tectonics and landscape evolution
Transform faults
Volcanic arc processes

VOLCANOLOGY
Atmospheric effects (volcano)
Calderas
Effusive volcanism
Eruption mechanisms and flow emplacement
Experimental volcanism
Explosive volcanism
Lava rheology and morphology
Magma chamber processes
Magma genesis and partial melting
Magma migration and fragmentation
Mud volcanism
Physics and chemistry of magma bodies
Physics of magma and magma bodies
Planetary volcanism
Pluton emplacement
Remote sensing of volcanoes
Subaqueous volcanism
Tephrochronology
Volcanic gases
Volcanic hazards and risks
Volcaniclastic deposits
Volcano/climate interactions
Volcano monitoring
Volcano seismology